Contents

Handbook of Time Series Analysis. Björn Schelter, Matthias Winterhalder, Jens Timmer

ISBN: ??????????????

10 Synchronization Analysis and Recurrence in Complex Systems

M. C. Romano, M. Thiel, Jürgen Kurths, M. Rolfs, R. Engbert, and R. Kliegl

We discuss an approach to detect and quantify phase synchronization in the case of coupled non-phase-coherent oscillators, which is based on the recurrence properties of the underlying system. First, we present an index which detects phase synchronization without computing the phase directly. We show that this index is also appropriate for non-phase-coherent systems, i.e., systems with a rather broad power spectrum. Furthermore, we illustrate the applicability of this index for time series strongly contaminated by noise.

Second, we present an algorithm, which is also based on recurrence to generate surrogates to test for phase synchronization. The generated surrogates correspond to independent copies of the underlying system. Hence, computing a phase synchronization index between one observed oscillator and the surrogate of the second oscillator, we can test for phase synchronization.

Finally, we apply the recurrence-based index, as well as the recurrence-based surrogates to fixational eye movements and find strong indications that both the left and right fixational eye movements are synchronized.

Author: Please check your address carefully. Please provide complete address (full Christian and family name, institutional affiliation, correct address incl. zip-code, and e-mail) to be inserted into the List of Contributors at the beginning of the book.

10.1 Introduction

The study of synchronization goes back to the seventeenth century and begins with the analysis of synchronization of nonlinear periodic systems. The synchronization phenomenon was probably discovered first by Huygens in 1673, who noticed that two pendulum clocks that hang on the same beam can synchronize. This discovery can be considered as the beginning of Nonlinear Science. The synchronization of the flashing of fireflies, the peculiarities of adjacent organ pipes which can almost annihilate each other or speak in unison, or the synchronization of diodes are other well known examples.

However, the research of synchronization in complex systems did not begin until the end of the eighties. It has been studied extensively during the last years [1–4], as this phenomenon has found numerous applications in natural (cardiorespiration, Parkinson patients, ecology, El Niño-Monsoon, etc.) [5–10] and engineering (lasers, plasma, tubes, etc.) systems [11–13]. Two systems are

Handbook of Time Series Analysis. Björn Schelter, Matthias Winterhalder, Jens Timmer

ISBN: ??????????????

said to be phase synchronized when their respective frequencies and phases are locked. Note that synchronization is a process (of adapting rhythms) and not a state. Till now phase synchronization (PS) of chaotic systems has been mainly observed for attractors with rather coherent phase dynamics. These attractors have a relatively simple topology of oscillations and a well-pronounced peak in the power spectrum, which allows to introduce the phase and the characteristic frequency of motions, Eq. (10.2). However, some difficulties appear when dealing with non-coherent attractors characterized by a rather broad band power spectra. Then it might not be straightforward to define a phase of the oscillations, and in general no single characteristic time scale exists. In contrast to phase coherent attractors, it is quite unclear whether some phase synchronized state can be achieved (Fig. 10.1).

To treat this problem, we propose a method based on another basic property of complex chaotic systems: recurrences in phase space. The concept of recurrence in dynamical systems goes back to Poincaré [14], when he proved that after a sufficiently long time interval, the trajectory of an isolated mechanical system will return arbitrarily close to each former point of its route. We will show that the concept of recurrence allows to detect indirectly synchronization and works even in the case of noisy non-phase-coherent oscillators. Instead of defining directly the phase, we consider the coincidence of certain recurrence structures of both coupled subsystems. By means of this comparison we are able to detect synchronization in complex systems.

Another important problem in the synchronization analysis is that even though the synchronization measures may be normalized, experimental time series often yield values which are not at the borders of the interval and hence are difficult to interpret. This problem can be overcome if the coupling strength between the two systems can be varied systematically and a rather large change in the measure can be observed, i.e., we have a so called active experiment [1–4]. However, there are other kind of experiments (passive ones), in which it is not possible to change the coupling strength systematically, e.g., the synchronization of the heart beats of a mother with her fetus [15]. In some cases, this problem has been tackled by interchanging the pairs of oscillators [15], for example the EEGs of other pregnant women were used as "natural surrogates." These surrogates are independent and hence not in PS with the original system. Hence, if the synchronization index obtained with the original data is not significantly higher than the index obtained with the natural surrogates, there is no sufficient evidence to claim synchronization. But even this rather innovative approach has some drawbacks. The natural variability and also the frequency of the heart beats of the surrogate mothers are usually lightly different from the ones of the real mother. Furthermore, the data acquisition can be expensive and at least in some cases problematic or even impossible (e.g., geophysical time series). In these cases it would be convenient to perform a hypothesis test based on surrogates generated by a mathematical algorithm.

Therefore, we present a technique for the generation of surrogates, which is based on the recurrences of a system. These surrogates mimic the dynamical behavior of the system. Then, computing the synchronization index between one subsystem of the original system and the other subsystem of the surrogate, and comparing it with the synchronization index obtained for the original system, we can test for PS.

In Section 10.2, we introduce the concept of recurrence, as well as the synchronization index based on the recurrence properties of the system. In Section 10.3 we show how to detect another kind of synchronization, namely generalized synchronization (GS) by means of recurrences and in Section 10.4 we show that the recurrence-based indices indicate the transition to PS and GS in accordance with other known theoretical methods. In Section 10.5 we present the twin surrogates technique and apply it to test for synchronization in the paradigmatic two coupled Rössler systems. In Section 10.6 we show an application of the recurrence-based index and surrogates to measured physiological data, namely fixational eye movements.

10.2 Phase Synchronization by Means of Recurrences

First, we exemplify the problem of defining the phase in systems with rather broad power spectrum by the paradigmatic system of two coupled nonidentical Rössler oscillators

$$\begin{aligned} \dot{x}_{1,2} &= -\omega_{1,2} y_{1,2} - z_{1,2} \,, \\ \dot{y}_{1,2} &= \omega_{1,2} x_{1,2} + a y_{1,2} + \mu(y_{2,1} - y_{1,2}) \,, \\ \dot{z}_{1,2} &= 0.1 + z_{1,2}(x_{1,2} - 8.5) \,, \end{aligned} \tag{10.1}$$

where μ is the coupling strength and $\omega_{1,2}$ determine the mean intrinsic frequency of the (uncoupled) oscillators in the case of phase coherent attractors. In our simulations we take $\omega_1 = 0.98$ and $\omega_2 = 1.02$. The parameter $a \in [0.15 : 0.3]$ governs the topology of the chaotic attractor. When a is below a critical value a_c ($a_c \approx 0.186$ for $\omega_1 = 0.98$ and $a_c \approx 0.195$ for $\omega_2 = 1.02$), the chaotic trajectories always cycle around the unstable fixed point $(x_0, y_0) \approx (0, 0)$ in the (x, y) subspace, i.e., $\max(y) > y_0$ (Fig. 10.1(a)). In this case, simply the rotation angle

$$\phi = \arctan \frac{y}{x} \tag{10.2}$$

can be defined as the phase, which increases almost uniformly. The oscillator has a coherent phase dynamics, i.e., the diffusion of the phase dynamics is very low (10^{-5} to 10^{-4}). In this case, other phase definitions, e.g., based on the Hilbert transform or on the Poincaré section, yield equivalent results [1–4]. However, beyond the critical value a_c, the trajectories no longer always completely cycle around (x_0, y_0), and some $\max(y) < y_0$ occur, which are associated with faster returns of the orbits; the attractor becomes a funnel one. Such earlier returns in

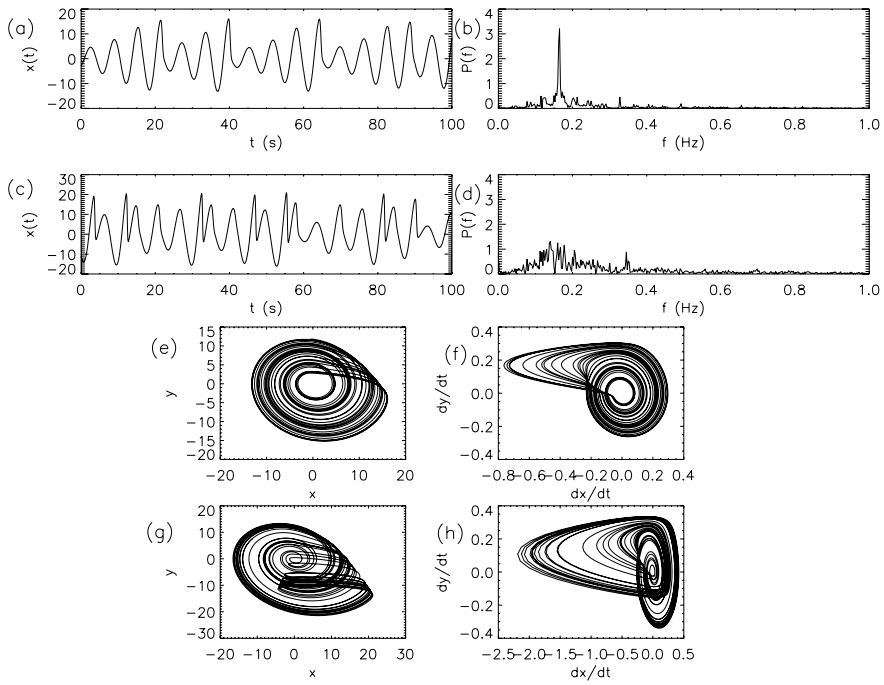

Fig. 10.1: (a,c) Segment of the x_1-component of the trajectory of the Rössler systems, Eq. (10.1). (b,d) periodogram of the x-component of the trajectory. (e,g) projection of the attractor onto the (x, y) plane. (g,h) projection onto the $(\dot{x}, \dot{y})$ plane. (a,b,e,f) computed for $a = 0.16$ and (c,d,g,h) computed for $a = 0.2925$.

the funnel attractor happen more frequently with increasing a (Fig. 10.1(b)). It is clear that for the funnel attractors, usual (and rather simple) definitions of phase, such as Eq. (10.2), are no longer applicable [1–4].

Rosenblum et al. have proposed in [16] to use an ensemble of phase coherent oscillators which is driven by the non-phase-coherent oscillator in order to estimate the frequency of the last, and hence detect PS in such kind of systems. However, depending on the component one uses to couple the non-phase-coherent oscillator to the coherent ones, the result of the obtained frequency can be different.

Furthermore, Osipov et al. [17] have proposed another approach which is based on the general idea of the curvature of an arbitrary curve [18]. For any two-dimensional curve $\mathbf{r}_1 = (u, v)$ the angle velocity at each point is $\nu = \frac{ds}{dt}/R$, where $ds/dt = \sqrt{\dot{u}^2 + \dot{v}^2}$ is the velocity along the curve and $R = (\dot{u}^2 + \dot{v}^2)^{3/2}/[\dot{v}\ddot{u} - \ddot{v}\dot{u}]$ is the curvature. If $R > 0$ at each point, then $\nu = \frac{d\phi}{dt} = \frac{\dot{v}\ddot{u} - \ddot{v}\dot{u}}{\dot{u}^2 + \dot{v}^2}$ is always positive and therefore the variable ϕ defined as $\phi = \int \nu \, dt = \arctan \frac{\dot{v}}{\dot{u}}$, is a monotonically growing angle function of time and can be considered as a phase

of the oscillations. Geometrically it means that the projection $\mathbf{r}_2 = (\dot{u}, \dot{v})$ is a curve cycling monotonically around a certain point.

These definitions of ϕ and ν hold in general for any dynamical system if the projection of the phase trajectory onto some plane is a curve with a positive curvature. This approach is applicable to a large variety of chaotic oscillators, such as the Lorenz system [19], the Chua circuit [20] or the model of an ideal four-level laser with periodic pump modulation [21].

This is clear for phase-coherent as well as funnel attractors in the Rössler oscillator. Here projections of chaotic trajectories on the plane $(\dot{x}, \dot{y})$ always rotate around the origin (Fig. 10.1(c) and (d)) and the phase can be defined as

$$\phi = \arctan \frac{\dot{y}}{\dot{x}} \,. \tag{10.3}$$

We have to note that for funnel-like chaotic attractors the coupling may change their topology. As a consequence the strong cyclic structure of orbits projection in the $(\dot{x}, \dot{y})$-plane may be destroyed and the phase measurement by Eq. (10.3) fails occasionally for intermediate values of coupling. But for small coupling and for coupling near the transition to PS, the phase is well-defined by Eq. (10.3) [22].

We consider two criteria to detect the existence of PS: Locking of the mean frequencies $\Omega_1 = \langle \nu_1 \rangle = \Omega_2 = \langle \nu_2 \rangle$, and locking of the phase $|\phi_2(t) - \phi_1(t)| \leqslant$ const (we restrict here to $1:1$ synchronization). Applying the new definition of the phase Eq. (10.3) to the system defined by Eq. (10.1) for $a = 0.2925$ (strongly noncoherent) and $\mu = 0.179$, one obtains the phase difference represented in Fig. 10.2.

We find two large plateaus in the evolution of the difference of the phases with time, i.e., we detect PS, but we also find a phase slip associated to a different number of oscillations in the two oscillators in the represented period of time. This means, we observe the rare occurrence of phase slip. It is interesting to note that in this system PS occurs after one of the positive Lyapunov exponents passes to negative values, i.e., it is also a transition to generalized chaotic synchronization (GS).

Although this approach works well in non-phase-coherent model systems, we have to consider that one is often confronted with the computation of the phase in experimental time series, which are usually corrupted by noise. In this case, some difficulties may appear when computing the phase by Eq. (10.3), because derivatives are involved in its definition.

Hence, we propose a different approach based on recurrences in phase space to detect PS indirectly. We define a recurrence of the trajectory of a dynamical system $\{\mathbf{x}(i)\}_{i=1}^{N}$ in the following way: We say that the trajectory has returned at time $t = j\delta t$ to the former point in phase space visited at $t = i\delta t$ if

$$R_{i,j}^{(\varepsilon)} = \Theta(\varepsilon - \|\mathbf{x}(i) - \mathbf{x}(j)\|) = 1 \,, \tag{10.4}$$

where ε is a pre-defined threshold, $\Theta(.)$ is the Heaviside function and δt is the sampling rate. A "1" in the matrix at i, j means that $\mathbf{x}(i)$ and $\mathbf{x}(i)$ are neighbor-

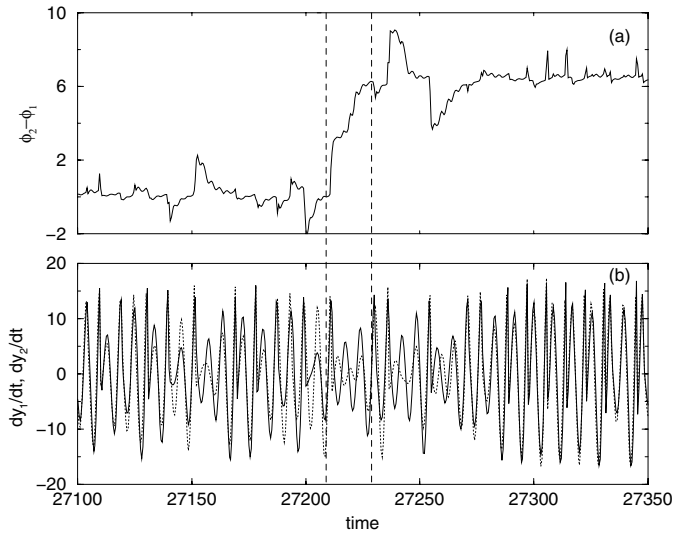

Fig. 10.2: (a) Time evolution of phase difference of the system of Eq. (10.1). (b) Variables $\dot{y}_{1,2}$ in system (10.1) for $a = 0.2925$ and $\mu = 0.179$. Solid and dotted lines correspond to the first and the second oscillator, respectively. In the time interval between dashed lines the first oscillator produces four rotations in the $(\dot{x}_1, \dot{y}_1)$-plane around the origin, but the second one generates only three rotations, which leads to a phase slip in (a).

ing, a "0" that they are not. The black and white representation of this binary matrix is called recurrence plot (RP). This method has been intensively studied in the last years: Different measures of complexity have been proposed based on the structures obtained in the RP and have found numerous applications in, e.g., physiology and earth science [23–27]. Furthermore, it has been even shown that some dynamical invariants can be estimated by means of the recurrence structures [28].

Based on this definition of recurrence, we want to tackle the problem of performing a synchronization analysis in the case of non-phase-coherent systems. We avoid the direct definition of the phase and instead use the recurrence properties of the systems in the following way: The probability $P^{(\varepsilon)}(\tau)$ that the system returns to the neighborhood of a former point $\mathbf{x}(i)$ of the trajectory[1] after τ time steps can be estimated as follows:

$$\hat{P}^{(\varepsilon)}(\tau) = \frac{1}{N-\tau} \sum_{i=1}^{N-\tau} \Theta(\varepsilon - \|\mathbf{x}(i) - \mathbf{x}(i+\tau)\|) = \frac{1}{N-\tau} \sum_{i=1}^{N-\tau} R^{(\varepsilon)}_{i,i+\tau} \,. \qquad (10.5)$$

This function can be regarded as a generalized autocorrelation function, as it also describes higher order correlations between the points of the trajectory in

[1] The neighborhood is defined as a box of size ε centered at $\mathbf{x}(i)$, as we use the maximum norm.

dependence on the time delay τ. A further advantage with respect to the linear autocorrelation function is that $\hat{P}^{(\varepsilon)}(\tau)$ is defined for a trajectory in phase space and not only for a single observable of the system's trajectory. Further, we have recently shown that it is possible to reconstruct the attractor by only considering the recurrences of single components of the system [29] and it is also possible to estimate dynamical invariants of the system (e.g., entropies and dimensions) by means of recurrences in phase space [28]. Hence, the recurrences of the system in phase space contain information about higher order dependencies within the components of the system.

For a periodic system with period length T in a two-dimensional phase space, it can be easily shown that

$$P(\tau) = \lim_{\varepsilon \to 0} \hat{P}^{(\varepsilon)}(\tau) = \begin{cases} 1 & \tau = T \\ 0 & \text{otherwise}\,. \end{cases}$$

For coherent chaotic oscillators, such as Eq. (10.1) for $a = 0.16$, $\hat{P}^{(\varepsilon)}(\tau)$ has well-expressed local maxima at multiples of the mean period, but the probability of recurrence after one or more rotations around the fixed point is less than one (Fig. 10.5).

Analyzing the probability of recurrence, it is possible to detect PS for non-phase-coherent oscillators, too. This approach is based on the following idea: Originally, a phase ϕ is assigned to a periodic trajectory $\mathbf{x}$ in phase space, by projecting the trajectory onto a plane and choosing an origin, around which the trajectory oscillates all the time. Then an increment of 2π is assigned to ϕ, when the point of the trajectory has returned to its starting position, i.e., when $\|\mathbf{x}(t + T) - \mathbf{x}(t)\| = 0$. Analogously to the case of a periodic system, we can refer an increment of 2π to ϕ to a complex nonperiodic trajectory $\mathbf{x}(t)$, when $\|\mathbf{x}(t + T) - \mathbf{x}(t)\| \sim 0$, or equivalently when $\|\mathbf{x}(t + T) - \mathbf{x}(t)\| < \varepsilon$, where ε is a predefined threshold. That means, a recurrence $R^{(\varepsilon)}_{t,t+\tau} = 1$ can be interpreted as an increment of 2π of the phase in the time interval τ[2].

$\hat{P}^{(\varepsilon)}(\tau)$ can be viewed as a statistical measure on how often ϕ in the original phase space has increased by 2π or multiples of 2π within the time interval τ. If two systems are in PS, in the mean, the phases of both systems increase by $k \cdot 2\pi$, with k a natural number, within the same time interval τ. Hence, looking at the coincidence of the positions of the maxima of $\hat{P}^{(\varepsilon)}(\tau)$ for both systems, we can quantitatively identify PS (from now on, we omit (ε) and $\hat{}$ in $\hat{P}^{(\varepsilon)}(\tau)$ to simplify the notation). The proposed algorithm then consists of two steps:

- Compute $P_{1,2}(\tau)$ of both systems based on Eq. (10.5).
- Compute the cross-correlation coefficient between $P_1(\tau)$ and $P_2(\tau)$ (correlation between probabilities of recurrence, CPR)

$$\mathrm{CPR}^{1,2} = \frac{\langle \bar{P}_1(\tau)\bar{P}_2(\tau)\rangle_\tau}{\sigma_1\sigma_2}\,, \tag{10.6}$$

[2] This can be considered as an alternative definition of the phase to Eqs. (10.2) and (10.3).

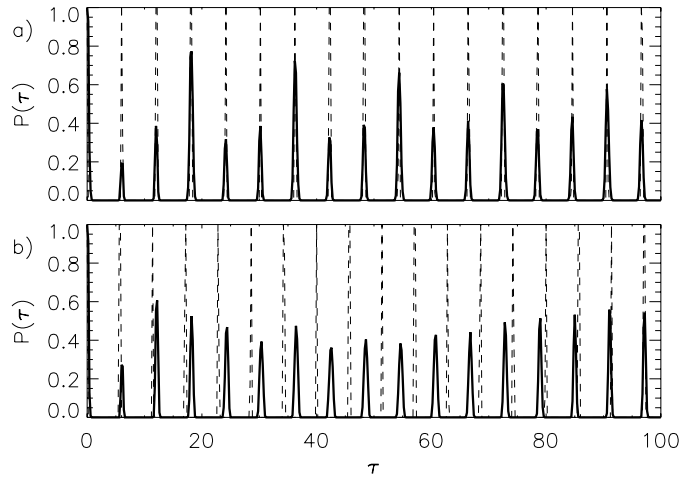

Fig. 10.3: $P(\tau)$ for a periodically driven Rössler (Eqs. (10.7)) in PS (a) and in non-PS (b). Solid line: $P(\tau)$ of the driven Rössler, dashed line: $P(\tau)$ of the periodic forcing.

where $\bar{P}_{1,2}$ means that the mean value has been subtracted and σ_1 and σ_2 are the standard deviations of $P_1(\tau)$ and $P_2(\tau)$, respectively.

If both systems are in PS, the probability of recurrence is maximal simultaneously and $CPR^{1,2} \sim 1$. In contrast, if the systems are not in PS, the maxima of the probability of recurrence do not occur jointly and expect low values of $CPR^{1,2}$.

10.2.1 Examples of Application

In this section we exemplify the application of CPR to detect PS for four prototypical chaotic systems. The number of data points used for the analysis presented here is 5000.

1. We start with the periodically driven Rössler system [1–4]

$$\begin{aligned} \dot{x} &= -y - z + \mu\cos(\omega t) \\ \dot{y} &= x + 0.15y \\ \dot{z} &= 0.4 + z(x - 8.5)\,. \end{aligned} \tag{10.7}$$

For the frequency $\omega = 1.04$ and the coupling strength $\mu = 0.16$, the periodic forcing locks the frequency of the Rössler system. This can be clearly seen in Fig. 10.3(a). The position of the maxima coincide. The value of the recurrence-based PS index (Eq. (10.6)) is $CPR = 0.862$.

For the parameters $\omega = 1.1$ and $\mu = 0.16$, the periodic forcing does not synchronize the Rössler system. Hence, the joint probability of recurrence is very low, which is reflected in the drift of the peaks of the corresponding $P(\tau)$ (Fig. 10.3(b)). In this case, $CPR = -0.00241$.

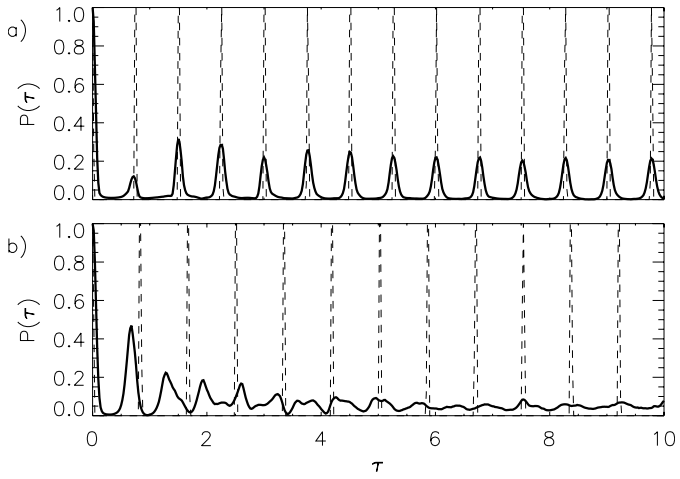

Fig. 10.4: $P(\tau)$ for a periodically driven Lorenz in PS (a) and in non-PS (b). Solid line: $P(\tau)$ of the driven Lorenz, dashed line: $P(\tau)$ of the periodic forcing.

2. We continue our considerations with the periodically driven Lorenz system for the standard parameters

$$\begin{aligned} \dot{x} &= 10(y - x) \\ \dot{y} &= 28x - y - xz \\ \dot{z} &= -8/3z + xy + \mu\cos(\omega t)\,. \end{aligned} \tag{10.8}$$

   In Fig. 10.4(a) the probabilities of recurrence $P(\tau)$ in the PS case ($\mu = 10$, $\omega = 8.35$) are represented. We see that the position of the local maxima of the Lorenz oscillator coincide with the ones of the periodic forcing. However, the local maxima are not as high as in the case of the Rössler system, and they are broader. This reflects the effective noise which is intrinsic in the Lorenz system [1–4]. Therefore, the phase synchronization is not perfect: An exact frequency locking between the periodic forcing and the driven Lorenz cannot be observed [30]. In this case, we obtain CPR $= 0.667$. In the non-PS case ($\mu = 10$, $\omega = 7.5$), we obtain CPR $= 0.147$ (Fig. 10.4(b)).

3. Next, we consider the case of two mutually coupled Rössler systems in the phase coherent regime, more precisely we analyze Eqs. (10.1) with $a = 0.16$. According to [17], for $\omega_1 = 0.98, \omega_2 = 1.02$ and $\mu = 0.05$ both systems are in PS. We observe that the local maxima of P_1 and P_2 occur at $\tau = n \cdot T$, where T is the mean period of both Rössler systems (Fig. 10.5(a)). The heights of the local maxima are in general different for both systems if they are only in PS and not in, e.g., complete synchronization or generalized synchronization. But the positions of the local maxima of $P(\tau)$ coincide. In this case, we obtain CPR $= 0.998$.

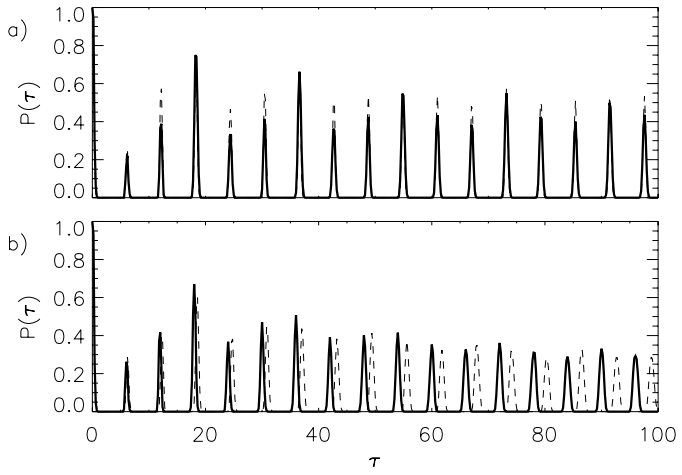

Fig. 10.5: $P(\tau)$ for two mutually coupled Rössler systems (Eqs. (10.1)) in phase coherent regime ($a = 0.16$) for $\mu = 0.05$ (a) and for $\mu = 0.02$ (b).

At a coupling strength of $\mu = 0.02$ the systems are not in PS and the positions of the maxima of $P(\tau)$ do not coincide anymore (Fig. 10.5(b)), clearly indicating that the frequencies are not locked. In this case, we obtain CPR $= 0.115$.

4. As a last example with simulated data, we analyze the challenging case of two mutually coupled Rössler systems in the funnel regime. Therefore, we study Eqs. (10.1) with $a = 0.2925$, $\omega_1 = 0.98$, and $\omega_2 = 1.02$. We analyze two different coupling strengths: $\mu = 0.2$ and $\mu = 0.05$. We observe that the structure of $P(\tau)$ in the funnel regime (Fig. 10.6) is rather different from the one in the phase coherent Rössler system (Fig. 10.5). The peaks in $P(\tau)$ are not as well pronounced as in the coherent regime, reflecting the different time scales that play a crucial role and the broad-band power spectrum of this system. However, we notice that for $\mu = 0.2$ the locations of the local maxima coincide for both oscillators (Fig. 10.6(a)), indicating PS, whereas for $\mu = 0.05$ the positions of the local maxima do not coincide anymore (Fig. 10.6(b)), indicating non-PS. These results are in accordance with [17].

   In the PS case, we obtain CPR $= 0.988$, and in the non-PS case, CPR $= 0.145$. Note that the position of the first peak in Fig. 10.6(b) coincides, although the oscillators are not in PS. This is due to the small frequency mismatch ($|\omega_1 - \omega_2| = 0.04$). However, by means of the index CPR we can distinguish rather well between both regimes.

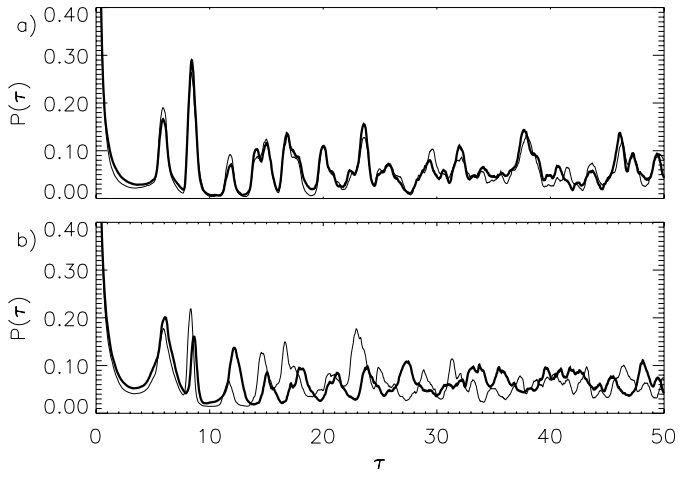

Fig. 10.6: $P(\tau)$ for two mutually coupled Rössler systems (Eqs. (10.1)) in funnel regime ($a = 0.2925$) for $\mu = 0.2$ (a) and for $\mu = 0.05$ (b). Bold line: $P_1(\tau)$, solid line: $P_2(\tau)$.

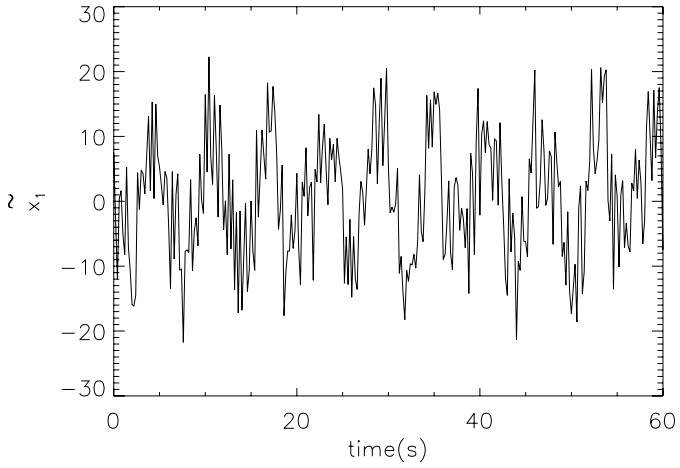

Fig. 10.7: First component x_1 of Eqs. (10.1) with 80% independent Gaussian noise (for $\mu = 0.05$). From the figure it is clearly recognizable that it is difficult to compute the phase by means of, e.g., the Hilbert transformation.

10.2.2 Influence of Noise

Measurement errors are omnipresent in experimental time series. Hence, it is necessary to analyze the influence of noise on CPR (correlation of probability of recurrence).

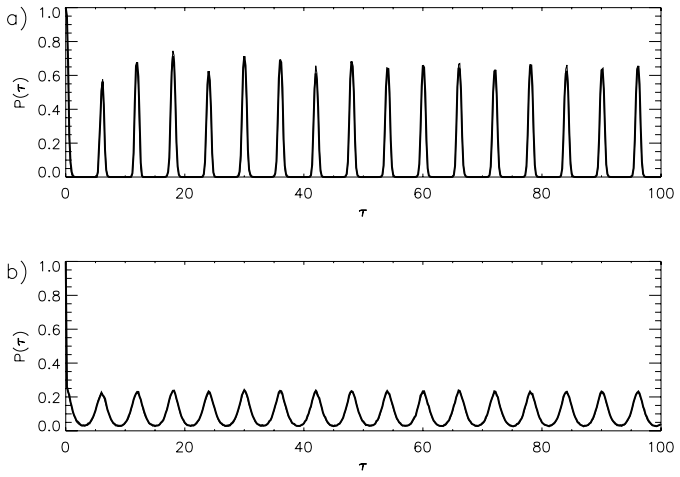

Fig. 10.8: Probabilities of recurrence for two coupled Rössler systems (Eqs. (10.1)) in PS ($\mu = 0.05$) without noise (a) and with 80% Gaussian observational noise (b). Bold line: subsystem 1, solid line: subsystem 2. Note that the position of the peaks of $P_1(\tau)$ and $P_2(\tau)$ coincide in both cases, and hence the solid line is hidden by the bold one.

First, we treat additive or observational white noise. We use Eqs. (10.1) with two different coupling strengths, so that we can compute the deviation which is caused by noise in the nonsynchronized and in the synchronized case.

We add independent Gaussian noise with standard deviation $\sigma_{\text{noise}} = \alpha\sigma_j$ to each coordinate j of the system, where σ_j is the standard deviation of the component j and α is the noise level. In Fig. 10.7 the "corrupted" x-component of the first Rössler subsystem $\tilde{x}_1(t) = x_1(t) + \alpha\sigma_1\eta(t)$ is represented. Herein $\eta(t)$ is a realization of Gaussian noise and $\alpha = 0.8$. From Fig. 10.7 it is obvious that it is difficult to compute the phase by means of, e.g., the Hilbert transformation for such a high noise level without filtering.

The choice of ε for the computation of $P_1(\tau)$ and $P_2(\tau)$ in the presence of noise is performed automatically by fixing the recurrence rate RR, i.e., the percentage of recurrence points in the recurrence matrix, Eq. (10.4). The results presented below were computed for RR $= 0.1$, but the results are rather independent of the choice of RR. However, RR should not be chosen too small if the level of noise is very high [23–27].

In order to compute CPR for the noisy oscillators, we calculate first the probabilities of recurrence $P_1(\tau)$ and $P_2(\tau)$ for coupling strengths $\mu = 0.05$ (PS, Fig. 10.8) and $\mu = 0.02$ (non-PS, Fig. 10.9).

We note that the peaks in $P_1(\tau)$ and $P_2(\tau)$ become lower and broader (Figs. 10.8(b) and 10.9(b)) compared with the noise free case (Figs. 10.8(a) and 10.9(a)), which is expected. However, despite of the large level of noise, the positions of the local

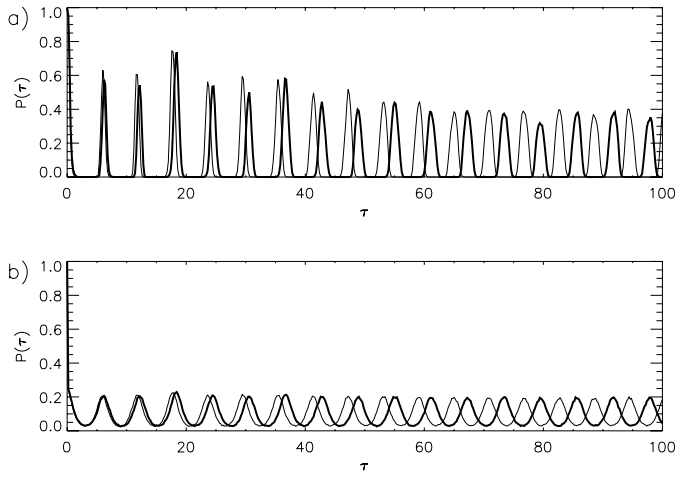

Fig. 10.9: Probabilities of recurrence for two coupled Rössler systems (Eqs. (10.1)) in non-PS ($\mu = 0.02$) without noise (a) and with 80% Gaussian observational noise (b). Bold line: subsystem 1, solid line: subsystem 2.

maxima coincide in the PS case, and they drift away in the non-PS case. This a convenient result, because we can still decide whether the oscillators are synchronized in a statistical sense or not. This is reflected in the obtained values for the CPR index: at a noise level of 80% noise, in the PS case the obtained value for CPR is exactly the same with and without noise, and in the non-PS case it is nearly the same (see Table 10.1). This shows that the index CPR for PS is very robust against observational noise.

Now, we analyze the influence of colored noise on the index CPR. We add a realization of colored noise with a very high noise amplitude to each component of the first system and another realization of colored noise with a smaller noise amplitude to each component of the second system (see Fig. 10.10(a) and (b) and the corresponding caption). Other methods fail determining the phase in this case, as for example the one presented in [17], because it requires the computation of the derivative of the time series, and due to the large level of noise, this is not possible. But by means of $P(\tau)$ we can distinguish PS from non-PS even in this case (Fig. 10.10(c) and (d)): We obtain CPR $= 0.0276$ for the non-PS case and CPR $= 0.530$ for the PS case.

Tab. 10.1: Index CPR for PS calculated for two coupled Rössler systems (10.1) with observational noise and without noise, for comparison.

μ	CPR (80% noise)	CPR (0% noise)
0.02 (non-PS)	0.149	0.115
0.05 (PS)	0.998	0.998

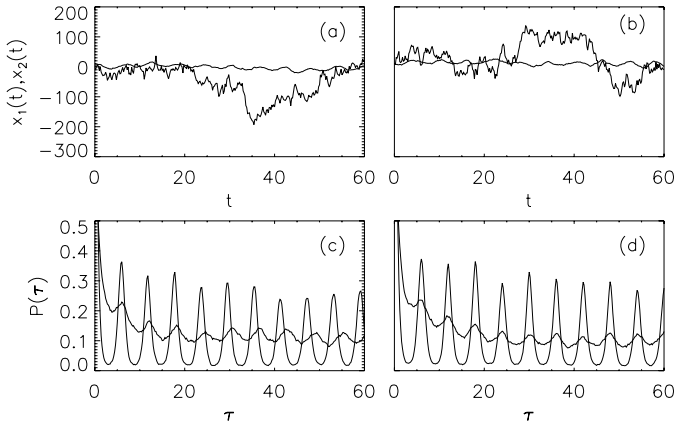

Fig. 10.10: (a,b) Segments of the x-components of the trajectories of two mutually coupled Rössler systems in phase coherent regime ($a = 0.16$) strongly contaminated by colored noise. A realization of $r_{t+1} = 0.99r_t + 10\eta_t$ and $s_{t+1} = 0.982s_t + \xi_t$ were respectively added to each component of the Rössler systems. (a) non-PS ($\mu = 0.02$). (b) PS ($\mu = 0.05$). (c) $P(\tau)$ for the two noisy Rössler for $\mu = 0.02$ (non-PS), (d) $P(\tau)$ for the two noisy Rössler for $\mu = 0.05$ (PS). Solid line: system 1, dashed line: system 2.

10.3 Generalized Synchronization and Recurrence

In this section we treat the issue of synchronization of coupled systems which are essentially different. This problem has been addressed first in [31, 32]. In this case, there is in general no trivial manifold in the phase space which attracts the systems' trajectories. It has been shown that these systems can synchronize in a more general way, namely $\mathbf{y} = \boldsymbol{\psi}(\mathbf{x})$, where $\boldsymbol{\psi}$ is a transformation which maps asymptotically the trajectories of $\mathbf{x}$ into the ones of the attractor $\mathbf{y}$. This kind of synchronization is called generalized synchronization (GS). The properties of the function $\boldsymbol{\psi}$ depend on the features of the systems $\mathbf{x}$ and $\mathbf{y}$, as well as on the attraction properties of the synchronization manifold $\mathbf{y} = \boldsymbol{\psi}(\mathbf{x})$ [33]. GS has been demonstrated in laboratory experiments for electronic circuits and laser systems [34–38] and has found applications for the the design of communication devices [39–43] and model verification and parameter estimations from time series [44, 45].

Some statistical measures have been introduced for the detection of GS, such as the method of mutual false nearest neighbors [31, 32] or variations of the method proposed and analyzed in [46–48], which are based on the squared mean distance and conditional distance between mutual nearest neighbors. Some other methods are based on the mutual predictability to detect dynamical interdependence [49, 50]. There, the nearest neighbors of each subsystem are computed separately in the respective (sub)state space.

In this section we present a criterion for the detection of GS, which exploits the relationship between the geometric connection of both systems and their recurrences. The connection between recurrences and GS is even more straightforward than the one between recurrences and PS. One can see that the concept of GS is linked to the one of recurrence, considering the fact that when $\mathbf{x}(t)$ and $\mathbf{y}(t)$ are in GS, two close states in the phase space of $\mathbf{x}$ correspond to two close states in the space of $\mathbf{y}$ [31, 32]. Hence, the "neighborhood identity" in phase space is preserved, i.e., they are topologically equivalent. Since the recurrence matrix (Eq. (10.4)) is nothing else but a record of the neighborhood of each point of the trajectory, one can conclude that two systems are in GS if their respective RPs are almost identical. Note that it is possible, under some conditions, to reconstruct the rank order of the time series considering only the information contained in the RP [29]. Therefore, we can use the recurrence properties to detect and quantify GS.

However, in practice we note that the recurrence matrices of two systems in GS are very similar, but not identical. Several reasons can be given to explain this observation: The finite ε-threshold, computational roundoff errors, measurements inaccuracies, etc. Hence, we construct an index that quantifies the degree of similarity between the respective recurrences of both systems. It compares the recurrences of each point of the first system with the local recurrences of the second system. This index has the advantage that it distinguishes rather well between non-PS, PS, and GS.

This index is based on the average probability of joint recurrence over time, given by

$$RR^{\mathbf{x},\mathbf{y}} = \frac{1}{N^2} \sum_{i,j=1}^{N} \Theta(\varepsilon^{\mathbf{x}} - \|\mathbf{x}_i - \mathbf{x}_j\|)\Theta(\varepsilon^{\mathbf{y}} - \|\mathbf{y}_i - \mathbf{y}_j\|)\,. \tag{10.9}$$

If both systems $\mathbf{x}$ and $\mathbf{y}$ are independent from each other, then the average probability of a joint recurrence[3] is given by $RR^{\mathbf{x},\mathbf{y}} = RR^{\mathbf{x}}RR^{\mathbf{y}}$. If the oscillators are on the other hand in GS, we expect an approximate identity of their respective recurrences, and hence $RR^{\mathbf{x},\mathbf{y}} = RR^{\mathbf{x}} = RR^{\mathbf{y}}$ [31, 32].

For the computation of the recurrence matrix in the case of essentially different systems that undergo GS, it is more appropriate to use a fixed number of nearest neighbors for each column in the matrix, following the idea presented in [46–48], than using a fixed threshold. This means that the threshold is different for each column in the RP, but subjected to the following condition $\sum_{j=1}^{N} \Theta(\varepsilon^i - \|\mathbf{x}_i - \mathbf{x}_j\|) = A \ \forall i$, where A is the fixed number of nearest neighbors. We can automatically fix the RR by means of $RR = AN/N^2 = A/N$, and using the same A for each subsystem $\mathbf{x}$ and $\mathbf{y}$, $RR^{\mathbf{x}} = RR^{\mathbf{y}} = RR$.

Hence, the coefficient $S = \frac{RR^{\mathbf{x},\mathbf{y}}}{RR}$ is an index for GS that varies from RR to 1: It is approximately RR for independent systems, and it is close to 1 for systems in GS. However, with the index S we would not detect lag synchronization (LS) ($\mathbf{y}(t+\tau) = \mathbf{x}(t)$). Since LS can be considered as a special case of GS [52], it would be desirable to have an index that also detects LS. For this reason, we include a time lag τ in the similarity and introduce the following quotient:

$$S(\tau) = \frac{1/N^2 \sum_{i,j}^{N} \Theta(\varepsilon_{\mathbf{x}}^i - lVert\mathbf{x}_i - \mathbf{x}_j\|)\Theta(\varepsilon_{\mathbf{y}}^i - \|\mathbf{y}_{i+\tau} - \mathbf{y}_{j+\tau}\|)}{RR}, \qquad (10.10)$$

where the thresholds $\varepsilon_{\mathbf{x}}^i$ and $\varepsilon_{\mathbf{y}}^i$ fullfil the following conditions: $\sum_{j=1}^{N} \Theta(\varepsilon_{\mathbf{x}}^i - \|\mathbf{x}_i - \mathbf{x}_j\|) = A$ and $\sum_{j=1}^{N} \Theta(\varepsilon_{\mathbf{y}}^i - \|\mathbf{y}_i - \mathbf{y}_j\|) = A \ \forall i$. Then, we choose the maximum value of $S(\tau)$ and normalize

$$JPR = \max_{\tau} \frac{S(\tau) - RR}{1 - RR}. \qquad (10.11)$$

We denote this index by JPR because it is based on the average joint probability of recurrence. Since $S(\tau)$ varies between RR and 1, JPR ranges from 0 to 1. The value of RR is a free parameter and its choice depends on the case under study. We consider rather low values of RR, e.g., 1% or 2% as appropriate.

10.3.1 Examples of Application

In this section we show two examples of chaotic systems that undergo GS and compute for them the recurrence-based index JPR (Eq. (10.11)).

1. First we consider a Lorenz system driven by a Rössler system. The equations of the driving system are

$$\begin{aligned} \dot{x}_1 &= 2 + x_1(x_2 - 4) \\ \dot{x}_2 &= -x_1 + x_3 \\ \dot{x}_3 &= x_2 + 0.45x_3 , \end{aligned} \qquad (10.12)$$

[3] Note that the average probability of a joint recurrence is the recurrence rate of the joint recurrence plot (JRP) [51].

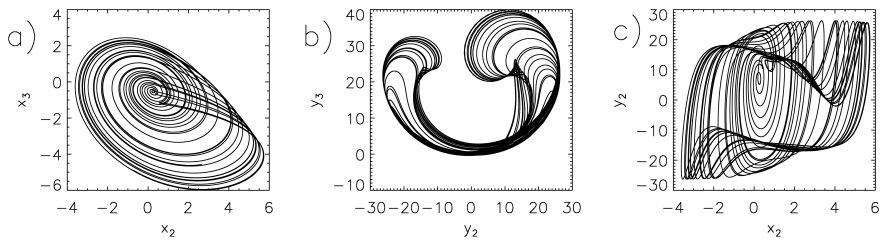

Fig. 10.11: Projection of the Rössler driving system (a), the driven Lorenz system (b) and the diagram x_2 versus y_2 of Eqs. (10.12) and (10.13) (c).

and following are the equations of the driven system:

$$\begin{aligned} \dot{y}_1 &= -\sigma(y_1 - y_2) \\ \dot{y}_2 &= r u(t) - y_2 - u(t) y_3 \\ \dot{y}_3 &= u(t) y_2 - b y_3 \,, \end{aligned} \tag{10.13}$$

where $u(t) = x_1(t) + x_2(t) + x_3(t)$ and the parameters were chosen as follows: $\sigma = 10$, $r = 28$, and $b = 2.666$. In [53] it was shown that the systems given by Eqs. (10.12) and (10.13) are in GS, since the driven Lorenz system is asymptotically stable.

To illustrate that they are completely different systems and that they are not in LS or even complete synchronized, Fig. 10.11 shows the projections of the system (Eqs. (10.12)) (a), of the system (Eqs. (10.13)) (b) and the x_2 versus y_2 diagram (c).

When dealing with experimental time series, usually only one observable of the system is available. Hence, we perform the analysis with just one component of each system to illustrate the applicability of the proposed method (we use 10 000 data points with a sampling time interval of 0.02 s). In this example, we take x_3 and y_3 as observables, respectively. Then, we reconstruct the phase space vectors using delay coordinates [54]. For the subsystem $\mathbf{x}$ we obtain the following embedding parameters [55]: delay time $\tau = 5$ and embedding dimension $m = 3$. For the subsystem $\mathbf{y}$ we find: $\tau = 5$ and $m = 7$. The corresponding RPs and JRP are represented in Fig. 10.12.

We see that despite of the essential difference between both subsystems, their RPs are very similar (Fig. 10.12(a) and (b)). Therefore, the structures are reflected also in the JRP and consequently, its recurrence rate is rather high. In this case, with the choice RR $= 0.02$ we obtain JPR $= 0.605$ (the value of JPR is similar for other choices of RR).

In order to illustrate the second case, where both subsystems are independent (Fig. 10.13), we compute the RP of the Rössler system (Eqs. (10.12)) and of

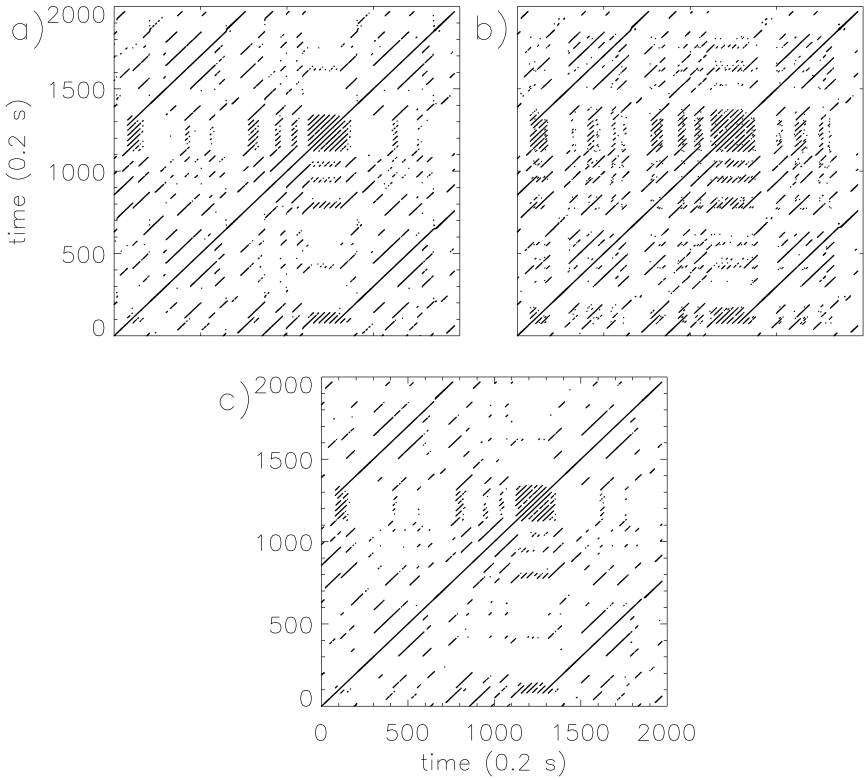

Fig. 10.12: (a) RP of the Rössler subsystem (Eqs. (10.12)). (b) RP of the driven Lorenz subsystem (Eqs. (10.13)). (c) JRP of whole system (Eqs. (10.12) and (10.13)).

the independent Lorenz system,[4] as well as their JRP (Fig. 10.14). Note that the mean probability over time for a joint recurrence is very small, as the JRP has almost no recurrence points. In this case, one obtains JPR $= 0.047$ using embedding parameters $\tau = 5$ and $m = 3$ for both systems, and RR $= 0.02$.

We placed the reference in a footnote. Please check.

For $\sigma = 10$ and $b = 8/3$ they display chaotic behavior.

2. Two mutually coupled Rössler systems (Eqs. (10.1)): for the coupling strength $\mu = 0.11$ both oscillators are in LS, as can be seen from Fig. 10.15.

   In this case, the RPs of both subsystems are obviously almost identical, except for a displacement on τ in the diagonal direction. Computing the index following Eq. (10.11), we obtain the value JPR $= 0.988$ (JPR in this case is not exactly 1), because we do not have perfect LS, i.e., $\mathbf{x}(t+\tau) \simeq \mathbf{y}(t)$ [52]). For a smaller coupling strength $\mu = 0.02$ the oscillators are not in LS anymore. The obtained value in this is case JPR $= 0.014$.

[4] The Lorenz equations are given by $\dot{x} = -\sigma x + \sigma y$, $\dot{y} = -xz + rx - y$, $\dot{z} = xy - bz$. For $\sigma = 10$ and $b = 8/3$ they display chaotic behavior.

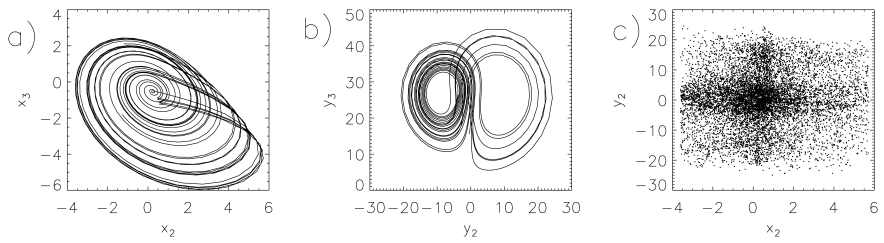

Fig. 10.13: Projection of the Rössler system (Eqs. (10.12)) (a), the independent Lorenz system (see footnote 4) (b) and the diagram x_2 versus y_2, where x_2 is the second component of the Rössler system and y_2 is the second component of the independent Lorenz system (c).

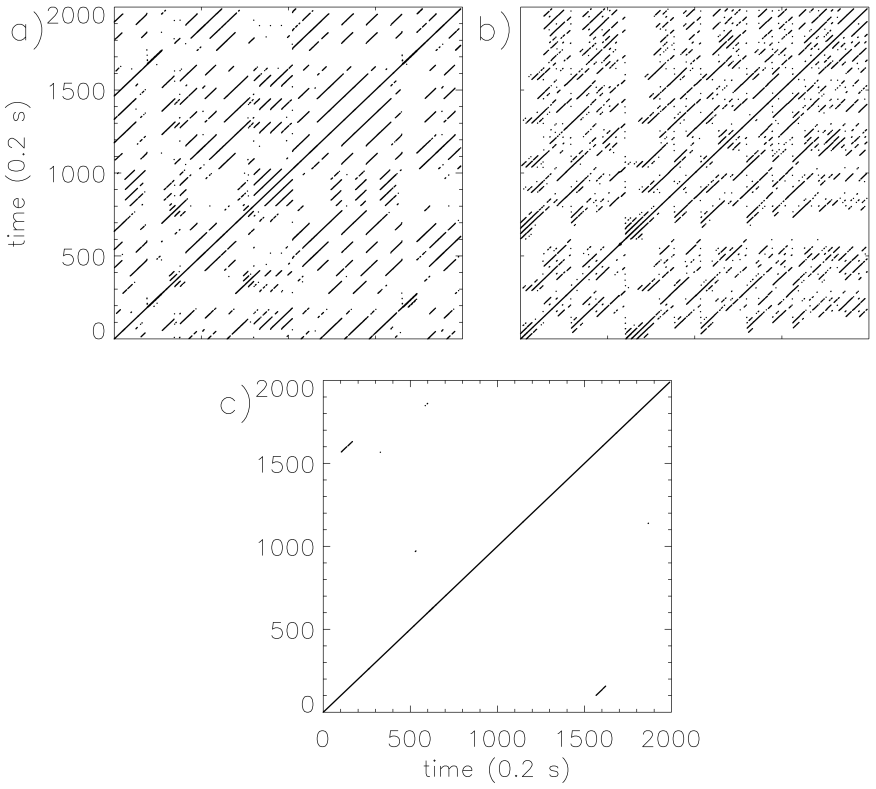

Fig. 10.14: (a) RP of the Rössler subsystem (Eqs. (10.12)). (b) RP of the independent Lorenz system (see footnote 4) (c) JRP of whole system.

10.4 Transitions to Synchronization

We have seen in the previous sections that the indices CPR and JPR clearly distinguish between oscillators in PS and oscillators which are not in PS, respectively of

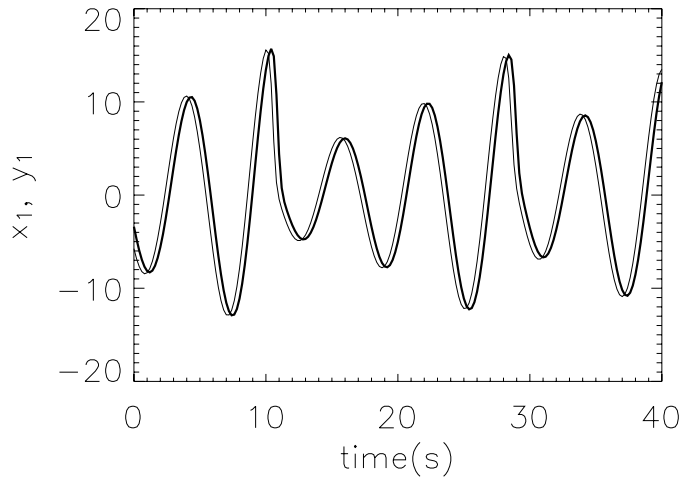

Fig. 10.15: Example of lag synchronization: It is clearly seen that x_1 (bold line) goes behind y_1 (solid line). It holds: $x_1(t+\tau) = y_1(t)$, with $\tau = 4$.

GS. On the other hand, the synchronization indices should not only distinguish between synchronized and nonsynchronized regimes, but also clearly indicate the onset of PS, respectively of GS.

In order to demonstrate that the recurrence-based indices fulfill this condition, we exemplify their application in the two cases: Two mutually coupled Rössler systems in a phase coherent regime and in a non-phase-coherent funnel regime (Eqs. (10.1)) with $a = 0.16$, respectively $a = 0.2925$). In both the cases we increase the coupling strength μ continuously and compute for each value of μ the indices CPR and JPR.

On the other hand, in the phase coherent case for a not too large but fixed frequency mismatch between both oscillators and increasing coupling strength, the transitions to PS and LS are reflected by the Lyapunov spectrum [1–4].[5] If both oscillators are not in PS, there are two zero Lyapunov exponents (λ_3 and λ_4), which correspond to the (almost) independent phases. Increasing the coupling strength, the fourth Lyapunov exponent λ_4 becomes negative (Fig. 10.16(c)), indicating the onset of PS. For higher coupling strengths, the second Lyapunov exponent λ_2 crosses zero, which indicates the establishment of a strong correlation between the amplitudes (Fig. 10.16(c)). This last transition occurs almost simultaneously with the onset of LS [52]. Therefore, we compute for our two examples also λ_2 and λ_4 in order to validate the results obtained with CPR and JPR.

In Fig. 10.16 the indices CPR (a) and JPR (b) are represented for increasing

[5] For other cases, e.g., for a fixed coupling strength and decreasing frequency mismatch, or for a large frequency mismatch and increasing coupling strength, the transition to PS is not always simply reflected in the Lyapunov spectrum [17, 51].

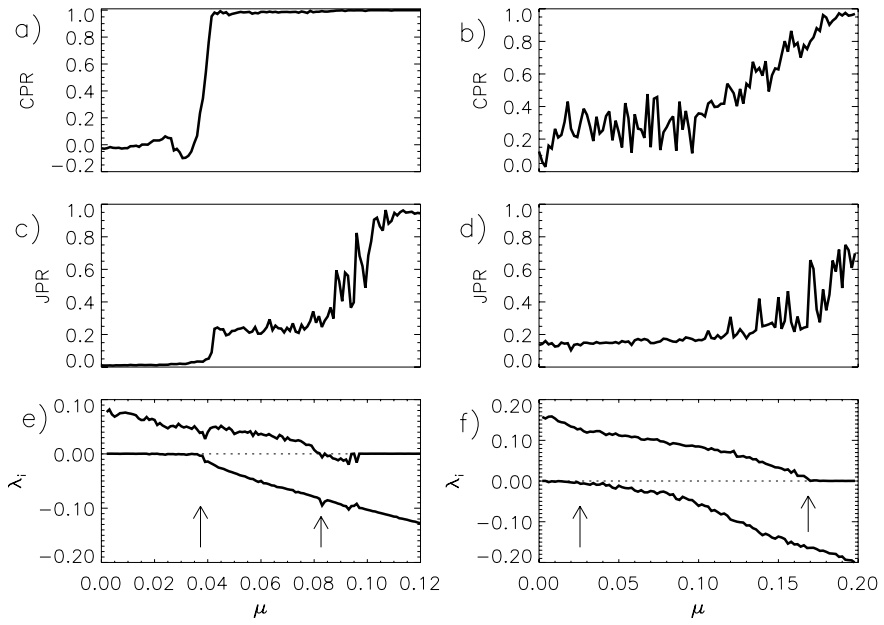

Fig. 10.16: CPR index, JPR index and λ_2 and λ_4 as functions of the coupling strength μ for two mutually coupled Rössler systems in phase coherent regime (a,c,e) and in funnel one (b,d,f). The dotted zero line in (e) and (f) is plotted to guide the eye. Here, we choose ε corresponding to 10% recurrence points in each RP.

coupling strength μ for the phase coherent case. In (c) λ_2 and λ_4 are shown in dependence on μ.

By means of CPR, the transition to PS is detected when CPR becomes of the order of 1. We see from Fig. 10.16(a) that the transition to PS occurs at approximately $\mu = 0.037$, in accordance with the transition of the fourth Lyapunov exponent λ_4 to negative values. The index JPR shows three plateaus in dependence on the coupling strength (Fig. 10.16(b)), indicating the onset of PS at the beginning of the second one. On the other hand, JPR clearly indicates the onset of LS because it becomes nearly one (third plateau) at approximately $\mu = 0.1$ (Fig. 10.16(b)), after the transition from hyperchaoticity to chaoticity, which takes place at approximately $\mu = 0.08$ (Fig. 10.16(c)). Between $\mu = 0.08$ and $\mu = 0.1$, the values of JPR have large fluctuations. This reflects the intermittent LS [1–4], where LS is interrupted by intermittent bursts of no synchronization.

Now we regard the more complex case of two coupled Rössler systems in the non-phase-coherent funnel regime, where the direct application of the Hilbert transformation is not possible [17]. In Fig. 10.16 the coefficients CPR and JPR are represented for this case in dependence on the coupling strength μ. Again, λ_2 and λ_4 are also shown (Fig. 10.16(f)).

First, note that for $\mu > 0.02$, λ_4 has already passed to negative values (Fig. 10.16(f)). However, CPR is still rather low, indicating that both oscillators are not in PS yet. CPR does not indicate PS until $\mu = 0.18$ (Fig. 10.16(d)), as found with other techniques [17]. Furthermore, we see from Fig. 10.16(f) that λ_2 vanishes at $\mu \sim 0.17$. This transition indicates that the amplitudes of both oscillators become highly correlated. At approximately the same coupling strength, JPR reaches rather high values, indicating the transition to GS (Fig. 10.16(e)). Then, according to the index CPR the transition to PS occurs after the onset of GS. This is a general result that holds for systems with a strong phase diffusion, as reported in [17]. For highly non-phase-coherent systems, there is more than one characteristic time scale. Hence, a rather high coupling strength is necessary in order to obtain phase locking of both oscillators. Hence, PS is not possible without a strong correlation in the amplitudes. PS for such non-phase-coherent systems has been recently found and analyzed in electrochemical oscillators [56] and in El Niño-Monsoon system [57].

Note that the synchronization indices presented in these sections based on recurrences are applicable to multivariate time series.

10.5 Twin Surrogates to Test for PS

As we have mentioned in Section 10.1, another essential problem in the synchronization analysis of observed time series is the construction of an appropriate hypothesis test to test for PS. Several approaches in this direction have been published [58, 59]. Usually, these are linear surrogates based on randomization of the Fourier phases [60, 61]. They mimic the individual spectra of the two components of the original bivariate series as well as their cross-spectrum, i.e., their linear properties, but not the higher order moments. In this case, the corresponding null hypothesis is that the putative synchronization in the underlying system can be explained by a bivariate linear stochastic process. The specificity of this test is not always satisfactory, because the concept of PS assumes the mutual adaption of self-sustained oscillators, i.e., nonlinear deterministic systems. On the other hand, pseudo-periodic surrogates (PPS) have been proposed to test the null hypothesis that an observed time series is consistent with an uncorrelated noise-driven periodic orbit [62]. The PPS are in a certain sense closer to the surrogates needed to test for PS as they correspond to trajectories of a deterministic system with noise, but they are still not appropriate to test for PS, as they are not able to model chaotic oscillators. Therefore, we present a technique for the generation of surrogates which are consistent with the null hypothesis of a trajectory of the same underlying system, but starting at different initial conditions [63]. Hence, they can also be used to test for PS in the case of chaotic oscillators.

The main idea consists in exchanging one original subsystem with one surrogate. Then, if the synchronization index obtained for the original system is not significantly different from the one computed for the exchanged subsystems, we

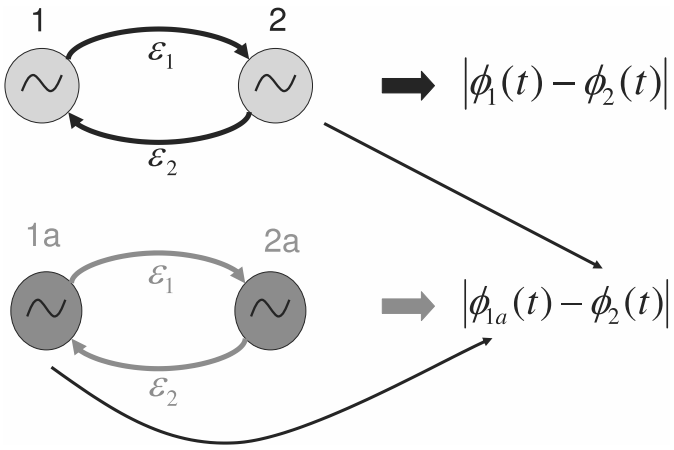

Fig. 10.17: This diagram represents the main idea using twin surrogates to test for PS.

have no sufficient evidence to claim synchronization (see Fig. 10.17). One could argue that the same can be achieved using different realizations of the same process and exchanging the subsystems. However, there are cases where it is not possible to measure several realizations, like, e.g., in geophysical systems.

The construction of the surrogates we present in this section is also based on the recurrence matrix (10.4). It is important to note that if the recurrence matrix is computed from a univariate time series, it contains all topological information about the underlying attractor, which therefore can be reconstructed from it [29].

Hence, a first idea for the generation of surrogates is to change the structures in a RP consistently with the ones produced by the underlying dynamical system. In this way one could reconstruct a new realization of the trajectory from the modified $R_{i,j}$. However, one cannot arbitrarily interchange columns in an RP, because such a modification changes the distribution of diagonal lines and hence the entropy and predictability of the system [28].

Therefore, we propose a modified approach. In general, in an RP there are identical columns, i.e., $R_{k,i} = R_{k,j}\ \forall k$ [28]. Thus, there are points which are not only neighbors (i.e., $\|\mathbf{x}_i - \mathbf{x}_j\|_\infty < \varepsilon$), but which also share the same neighborhood. Reconstructing the attractor from an RP, the respective neighborhoods of these points cannot help to distinguish them, i.e., from this point of view they are identical. This is why we will call them *twins*. Twins are special points of the time series as they are indistinguishable considering their neighborhoods but in general different and hence, have different pasts and—more important—different futures. The key idea of how to introduce the randomness needed for the generation of surrogates of a deterministic system is that one can jump randomly to one of the possible futures of the existing twins.

A surrogate trajectory $\mathbf{x}^s(i)$ of $\mathbf{x}(i)$ with $i = 1, \ldots, N$ is then generated in the following way:

1. Identify all pairs of twins.
2. Choose an arbitrary starting point, say $\mathbf{x}^s(1) = \mathbf{x}(k)$.
3. If $\mathbf{x}(k)$ has no twin, the next point of the surrogate trajectory is $\mathbf{x}^s(2) = \mathbf{x}(k+1)$.
4. If $\mathbf{x}(k)$ has a twin, say $\mathbf{x}(m)$, then one can go to either $\mathbf{x}(k+1)$ or to $\mathbf{x}(m+1)$, i.e., $\mathbf{x}^s(2) = \mathbf{x}(k+1)$ or $\mathbf{x}^s(2) = \mathbf{x}(m+1)$ with equal probability[6].

Steps three and four are then iterated until the surrogate time series has the same length as the original one.

This algorithm creates twin surrogates (TS) which are shadows of a (typical) trajectory of the system [64]. In the limit of an infinitely long original trajectory, its surrogates are characterized by the same dynamical invariants and the same attractor. However, if the measure of the attractor can be estimated from the observed finite trajectory reasonably well, its surrogates share the same statistics. Also their power spectra and correlation functions are consistent with the ones of the original system. TS do not only seem to give reasonable results for deterministic systems; the TS of for example an ARMA process also show the typical behavior of a linear Gaussian process.

Next, we use the TS to test for PS. The idea behind this approach is similar to the one by means of "natural surrogates" in the mother–fetus heartbeat synchronization [15]. Suppose that we have two coupled self-sustained oscillators $\mathbf{x}_1(t)$ and $\mathbf{x}_2(t)$. Then, we generate M TS of the joint system, i.e., $\mathbf{x}_1^{s_i}(t)$ and $\mathbf{x}_2^{s_i}(t)$, with $i = 1, \ldots, M$. These surrogates are independent copies of the joint system, i.e., trajectories of the whole system beginning at different initial conditions. Note that the coupling between $\mathbf{x}_1(t)$ and $\mathbf{x}_2(t)$ is also mimicked by the surrogates. Next, we compute the differences between the phases of the original system $\Delta\Phi(t) = \Phi_1(t) - \Phi_2(t)$ applying, e.g., the analytical signal approach [1–4] and compare them with $\Delta\Phi^{s_i}(t) = \Phi_1(t) - \Phi_2^{s_i}(t)$ (one can also consider $\Phi_1^{s_i}(t) - \Phi_2(t)$). Then, if $\Delta\Phi(t)$ does not differ significantly from $\Delta\Phi^{s_i}(t)$ with respect to some index for PS, the null hypothesis cannot be rejected and hence, we do not have enough evidence to state PS.

As a test case, we consider two nonidentical, mutually coupled Rössler oscillators

$$\begin{aligned} \dot{x}_{1,2} &= -(1 \pm \nu) y_{1,2} - z_{1,2} + \varepsilon(x_{2,1} - x_{1,2}), \\ \dot{y}_{1,2} &= (1 \pm \nu) x_1 + 0.15 y_{1,2}, \\ \dot{z}_{1,2} &= 0.2 + z_{1,2} + z_{1,2}(x_{1,2} - 10)\,, \end{aligned} \tag{10.14}$$

where $\nu = 0.015$ denotes the frequency mismatch. In this "active experiment", we vary the coupling strength ε from 0 to 0.08 and compute a PS index for the original trajectory for each value of ε. Next we generate 200 TS and compute the PS

[6] If triplets occur one proceeds analogously.

index between the measured first oscillator and the surrogates of the second one. As PS index we use the mean resultant length R of complex phase vectors [65, 66], which is motivated by Kuramoto's order parameter [67]

$$R = \left| \frac{1}{N} \sum_{t=1}^{N} \exp\bigl(i\Delta\Phi(t)\bigr) \right|. \tag{10.15}$$

It takes on values in the interval from 0 (non PS) to 1 (perfect PS) [65, 66]. Let R^{s_i} denote the PS index between the first oscillator and the surrogate i of the second one. To reject the null hypothesis at a significance value α, R must be larger than $(1-\alpha)\cdot 100$ percent of all R^{s_i}. Note that this corresponds to computing the significance level from the cumulative histogram at the level $(1-\alpha)$.

Figure 10.18(a) shows the results for R of the original system (bold line) and the 1% (solid) significance level. Figure 10.18(b) displays the difference between R of the original system and the 1%, 2% and 5% significance level. For $\varepsilon < 0.025$, R of the original system is, as expected, below the significance levels and hence the difference is negative, and for higher values of ε the curves cross (the difference becomes positive). This is in agreement with the criterion for PS via Lyapunov exponents λ_i [1–4]: λ_4 becomes negative at $\varepsilon \sim 0.028$ (Fig. 10.18(b)), which approximately coincides with the intersection of the curve of R for the original system and the significance level (zero-crossing of the curves in Fig. 10.18(b)). Therefore, we recognize successfully the PS region by means of the TS.

Note that also the significance limit increases when the transition to PS occurs (Fig. 10.18(a)). As the TS mimic both the linear and nonlinear characteristics of the system, the surrogates of the second oscillator have in the PS region the same mean frequency as the first original oscillator. Hence R^{s_i} is rather high. However, $\Phi_1(t)$ and $\Phi_2^{s_i}(t)$ do not adapt to each other, as they are independent. Hence, the value of R for the original system is significantly higher than the R^{s_i}. We state in conclusion that even though the obtained value for a normalized PS index is higher than 0.97 (right side of Fig. 10.18(a)), this does not offer conclusive evidence for PS. Hence, *the knowledge of the PS index alone does not provide sufficient evidence for PS*. Note that the more phase coherent the oscillators are, the more difficult it is to decide whether they are in PS or not. A certain phase diffusion, which allows to measure the adaptation of the phases of the interacting oscillators is necessary to detect PS. However, the test based on the TS reveals whether there is enough evidence for PS.

Next, we perform an analysis of the specificity and sensitivity of the test for $\varepsilon = 0$ and $\nu = 0$. For 100 random initial conditions of the Rössler system and a significance level of $\alpha = 1\%$, the null hypothesis was erroneously rejected only in 1 out of the 100 cases. This is a rather auspicious result, as due to the identical frequencies, it is extremely difficult to recognize that there is no PS in this case [68]. In the case of $\varepsilon = 0.02$ (e.g., no PS) and $\nu = 0.015$, there were no erroneous rejections of the null hypothesis. Finally, for PS ($\varepsilon = 0.045$ and

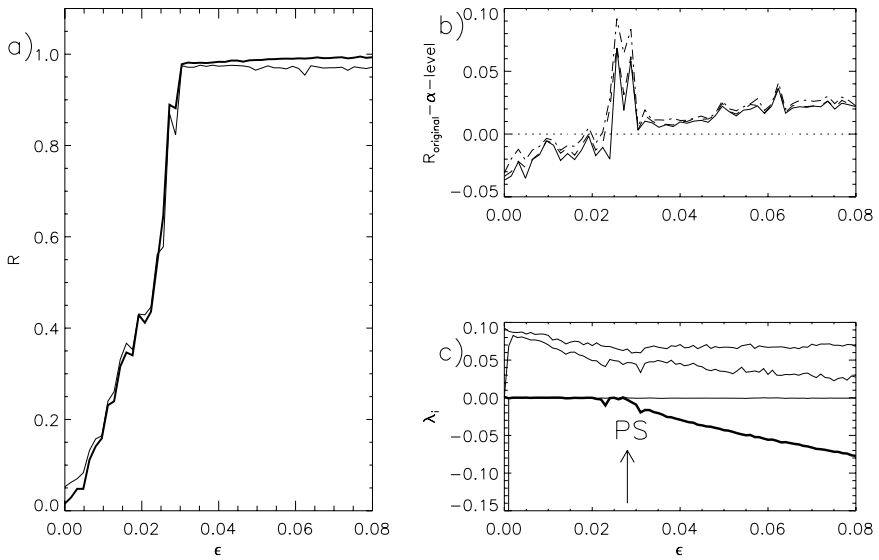

Fig. 10.18: (a) R of the original two mutually coupled Rössler systems with a frequency mismatch of $\nu = 0.015$ (bold) and significance level of 1% (solid). (b) Difference between R of the original data and significance level of 1% (solid), 2% (dashed) and 5% (dashed-dotted). The zero line is plotted (dotted) to guide the eye. (c) Four largest Lyapunov exponents for the six-dimensional system considered. λ_4 is highlighted and the arrow indicates the transition to PS.

$\nu = 0.015$), in all 100 test runs the null hypothesis was correctly rejected. These results indicate that the specificity and sensitivity of the test are good.

10.6 Application to Fixational Eye Movements

Next we apply the recurrence approach to check fixational movements of left and right eyes for PS. During fixation of a stationary target our eyes perform small involuntary and allegedly erratic movements to counteract retinal adaptation. If these eye movements are experimentally suppressed, retinal adaptation to the constant input induces very rapid perceptual fading [69, 70]. Moreover, statistical correlations show a timescale separation from persistence to antipersistence [71]. Persistence on the short timescale counteracts retinal fading, whereas antipersistence on the long timescale contributes to stability of ocular disparity. According to current textbook knowledge, the fixational movements of the left and right eyes are correlated very poorly at best [72]. Therefore, it is highly desirable to examine these processes from a perspective of PS. We analyze the data of two subjects. Each performed three trials, in which they fixated a small stimulus (black square on a white background, 3× pixels on a computer display) with a spatial extent of

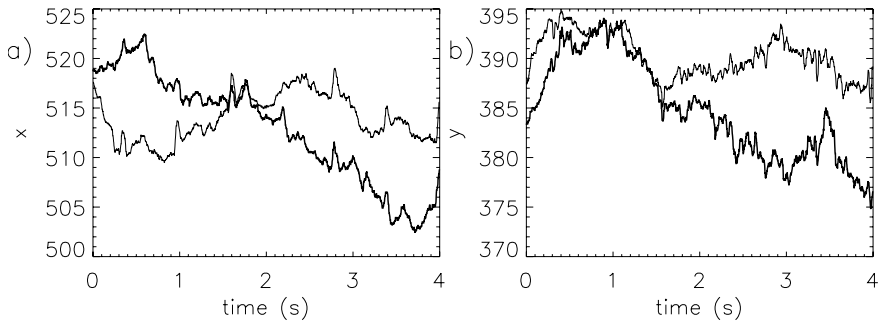

Fig. 10.19: Simultaneous recording of left (bold) and right (solid) fixational eye movements (a) horizontal component (b) vertical component.

0.12°, or 7.2 arc · min. Eye movements were recorded using an EyeLink-II system (SR Research, Osgoode, Ontario, Canada) with a sampling rate of 500 Hz and an instrument spatial resolution less than 0.005°. Figure 10.19 shows a segment of the horizontal (a) and vertical (b) component of the eye movements for one person.

The data were first high-pass filtered applying a difference filter $\tilde{x}(t) = x(t) - x(t-\tau)$ with $\tau = 40$ ms in order to eliminate the slow drift of the data. After this filtering, we find an oscillatory trajectory, which has maximum spectral power in the frequency range between 3 and 8 Hz (Fig. 10.20(a) and (b)). However, the trajectories of the eyes are rather noisy and non-phase-coherent. Therefore, it is cumbersome to estimate the phase of these data. Hence we apply the recurrence-based measure CPR introduced in Section 10.2 and we obtain the values displayed in the first column of Table 10.2. First, we observe that the variability between the different trials is smaller for the first participant as for the second one. Furthermore, the values of CPR are rather high for the first participant but not so high for the second one. Hence, a hypothesis test should be performed in order to get statistically significant results.

Therefore, we compute 200 twin surrogates of the left eye's trajectory. In Fig. 10.20(c) the horizontal component of one surrogate is represented. At a first glance, the characteristics of the original time series are well reproduced by the twin surrogate. In Fig. 10.20(d) the corresponding periodogram is displayed. It is also noteworthy that the structure of the original curve (Fig. 10.20(b)) is also qualitatively reproduced. The periodogram of the twin surrogate is of course not identical with the one of the original time series. This is consistent with the null hypothesis of another realization of the same underlying process, respectively another trajectory starting at different initial conditions of the same underlying dynamical system.

Now, we compute the recurrence-based synchronization index CPR^{s_i} between the twin surrogates of the left eye and the measured right eye's trajectory. In Fig. 10.21 the results of the test of one trial are visualized.

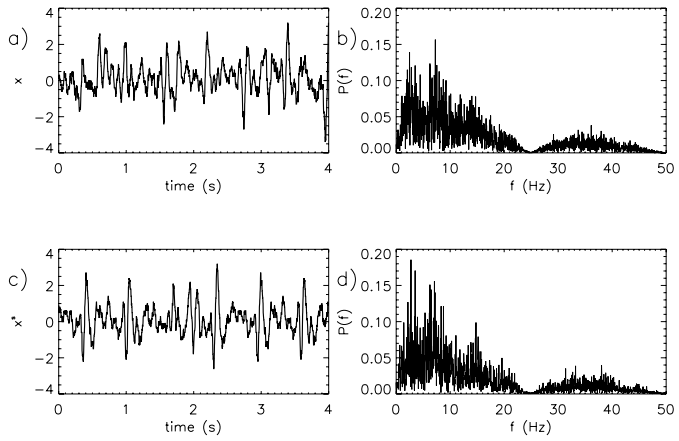

Fig. 10.20: Filtered horizontal component of the left eye of one participant (a) and its corresponding periodogram (b). In (c) the horizontal component of one surrogate of the left eye is represented and in (d) its corresponding periodogram.

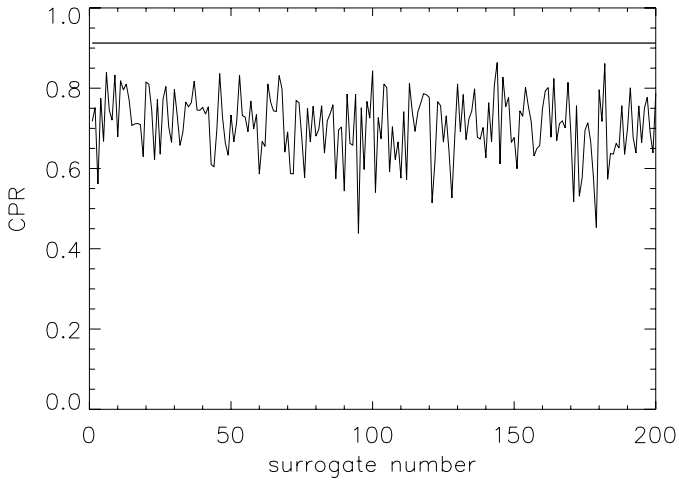

Fig. 10.21: Result of the test performed for one trial of one participant. The PS index for the original data (bold line) is significantly different from the one of the surrogates (solid).

The second column of Table 10.2 summarizes the results for both subjects and all trials.

In all cases, the PS index of the original data is significantly different from the ones of the surrogates, which strongly indicates that the concept of PS can be successfully applied to study the interaction between the trajectories of the left and

Tab. 10.2: Results for the test for PS between the trajectories of the left and right fixational eye movements performed for three trials for the two participants. Two hundred surrogates were used for the test. The null hypothesis was rejected in all cases at a 2% level.

Participant	CPR of the original data	Null hypothesis
M.R.	0.9112	Rejected
	0.9432	Rejected
	0.9264	Rejected
M.T.	0.6080	Rejected
	0.4844	Rejected
	0.3520	Rejected

right eyes during fixation. This result also suggests that the physiological mechanism in the brain that produces the fixational eye movements controls both eyes simultaneously, i.e., there might be only one center in the brain that produces the fixational movements in both eyes or a close link between two centers. Our finding of PS between left and right eyes is in good agreement with current knowledge of the physiology of the oculomotor circuitry. In a single-cell study, 66 % of abducens motor neurons fired in relation to the movements of either eye, while premotor neurons in the brainstem encode monocular movements [73]. Thus, motor neurons – as the final common pathway of neural control of eye movements – are candidates for the synchronization of left and right fixational movements. Furthermore, we are interested in whether the fixational movements in the horizontal and vertical direction of one eye are synchronized. Horizontal and vertical saccadic eye movements are controlled in two spatially distinct brainstem nuclei [74]. Therefore, we can expect that, on the level of fixational eye movements, horizontal and vertical components are independent. Applying the synchronization index CPR between the x- and y-component of the left eye of each participant for each trial and generate 200 surrogates of the two-dimensional trajectory of the left eye. Then we compare the synchronization index CPR^{s_i} between the original x-component and the y-component of the surrogates. We find in all but one cases that CPR is not significantly different from CPR^{s_i} (see Table 10.3). Hence, we do not have evidence to claim synchronization between the horizontal and vertical components of the eye movements, as expected.

10.7 Conclusions

In conclusion, we have presented solutions to two main problems of the synchronization analysis of measured time series: The detection of PS in non-phase-coherent systems and the hypothesis test for PS, which is interesting especially for passive experiments, where the coupling strength between the two subsystems cannot be varied systematically.

Tab. 10.3: Results for the test for PS between the horizontal and vertical components of fixational movements of one eye performed for three trials for the two participants. 200 surrogates were used for the test. In all cases but one, we failed to reject the null hypothesis at a 2 % level.

Participant	CPR of the original data	Null hypothesis
M.R.	0.3746	Not rejected
	0.6103	Not rejected
	0.4812	Rejected
M.T.	0.4681	Not rejected
	0.3194	Not rejected
	0.4172	Not rejected

We have given solutions to these two problems based on the concept of recurrence in phase space. First, we have shown that by means of the recurrence properties it is possible to detect indirectly PS even in the case of non-phase-coherent and strong noisy time series. Furthermore, it is also possible to detect GS by means of recurrences. Second, the method of twin surrogates has been presented, which is also based on recurrence, and we have shown that it can be used to test for PS.

We have used the well studied system of two mutually coupled Rössler oscillators in order to validate the techniques proposed. Furthermore, we have tested for PS in experiments of binocular fixational movements and found that the left and right eyes are in PS, in agreement with physiological results about the functional role of motor neurons in the final common pathway for the control of eye movements. Hence, we have shown that the techniques proposed are also applicable to rather noisy observed time series.

Acknowledgements

This work has been suported by the DFG Priority Program 1114 and the "Internationales Promotionskolleg—Helmholtz Center for the Study of Mind and Brain Dynamics" at the University of Potsdam.

Author: Please provide publisher and place in [3]

Author: Please update [63]

References

[1] M. Rosenblum, A. Pikovsky, and J. Kurths. *Phys. Rev. Lett.*, 76:1804, 1996.

[2] A. Pikovsky, M. Rosenblum, G. Osipov, and J. Kurths. *Physica D*, 104:219, 1997.

[3] A. Pikovsky, M. Rosenblum, and J. Kurths. *Synchronization*, volume 12 of *Cambridge Nonlinear Science Series*. 2001.

[4] S. Boccaletti, J. Kurths, G. V. Osipov, D. Valladares, and C. Zhou. *Phys. Rep.*, 366:1, 2002.

[5] R. C. Elson et al. *Phys. Rev. Lett.*, 81:5692, 1998.

[6] P. Tass et al. *Phys. Rev. Lett.*, 81:3291, 1998.

[7] C. M. Ticos et al. *Phys. Rev. Lett.*, 85:2929, 2000.

[8] V. Makarenko and R. Llinas. *Proc. Natl. Acad. Sci. USA*, 95:15474, 1998.

[9] B. Blasius, A. Huppert, and L. Stone. *Nature*, 399:354, 1999.

[10] C. Schäfer et al. *Nature*, 392:239, 1998.

[11] D. J. DeShazer et al. *Phys. Rev. Lett.*, 87:044101, 2001.

[12] S. Boccaletti et al. *Phys. Rev. Lett.*, 89:194101, 2002.

[13] I. Kiss and J. Hudson. *Phys. Rev. E*, 64:046215, 2001.

[14] H. Poincaré. *Acta Math.*, 13:1, 1890.

[15] P. Van Leeuwen et al. *BMC Physiol.*, 3:2, 2003.

[16] M. G. Rosenblum, A. S. Pikovsky, J. Kurths, G. V. Osipov, I. Z. Kiss, and J. L. Hudson. *Phys. Rev. Lett.*, 89:264102, 2002.

[17] G. V. Osipov, B. Hu, C. Zhou, M. V. Ivanchenko, and J. Kurths. *Phys. Rev. Lett.*, 91:024101, 2003.

[18] G. Fisher. *Plane Algebraic Curves*. American Mathematical Society, Providence, Rhode Island, 2001.

[19] C. Sparrow. *The Lorenz Equations: Bifurcations, Chaos, and Strange Attractors*. Springer, Berlin, Heidelberg, 1982.

[20] R. N. Madan. *Chua Circuit: A Paradigm for Chaos*. World Scientific, Singapore, 1993.

[21] W. Lauterborn, T. Kurz, and M. Wiesenfeldt. *Coherent Optics. Fundamentals and Applications*. Springer, Berlin, Heidelberg, New York, 1993.

[22] J. Y. Chen et al. *Phys. Rev. E*, 64:016212, 2001.

[23] J.-P. Eckmann, S. O. Kamphorst, and D. Ruelle. *Europhys. Lett.*, 4:973, 1987.

[24] C. L. Weber Jr. and J. P. Zbilut. *J. Appl. Physiol.*, 76:965, 1994.

[25] N. Marwan, N. Wessel, U. Meyerfeldt, A. Schirdewan, and J. Kurths. *Phys. Rev. E*, 66:026702, 2002.

[26] N. Marwan and J. Kurths. *Phys. Lett. A*, 302:299, 2002.

[27] M. Thiel et al. *Physica D*, 171:138, 2002.

[28] M. Thiel, M. C. Romano, P. Read, and J. Kurths. *Chaos*, 14:234, 2004.

[29] M. Thiel, M. C. Romano, and J. Kurths. *Phys. Lett. A*, 330:343, 2004.

[30] E.-H. Park, M. Zaks, and J. Kurths. *Phys. Rev. E*, 60:6627, 1999.

[31] V. S. Afraimovich, N. N. Verichev, and M. I. Rabinovich. *Izvestiya Vysshikh Uchebnykh Zavedenii Radiofizika*, 29:1050, 1986.

[32] N. F. Rulkov, M. M. Sushchik, L. S. Tsimring, and H. D. I. Abarbanel. *Phys. Rev. E*, 51 2:980, 1995.

[33] U. Parlitz and L. Kocarev. Synchronization of chaotic systems. In H. G. Schuster, editor, *Handbook of Chaos Control*. Wiley-VCH, Weinheim, 1999.

[34] L. M. Pecora and T. L. Carroll. *Phys. Rev. Lett.*, 64:821, 1990.

[35] K. M. Cuomo and A. V. Oppenheim. *Phy. Rev. Lett.*, 71:65, 1993.

[36] A. Kittel, A. Parisi, and K. Pyragas. *Physica D*, 112:459, 1998.

[37] G. D. Van Wiggeren and R. Roy. *Science*, 279:1198, 1998.

[38] K. Otsuka, R. Kawai, S.-L. Hwong, J.-Y. Ko, and J.-L. Chern. *Phys. Rev. Lett.*, 84:3049, 2000.

[39] C. W. Wu and L. O. Chua. *Int. J. Bif. Chaos*, 4:1979, 1994.

[40] T. L. Carroll and L. M. Pecora. *Physica D*, 67:126, 1993.

[41] L. Kocarev and U. Parlitz. *Phys. Rev. Lett.*, 74:5028, 1995.

[42] U. Parlitz, L. Kocarev, T. Stojanovski, and H. Preckel. *Phys. Rev. E*, 53:4351, 1996.

[43] L. Kocarev, K. S. Halle, K. Eckert, L. O. Chua, and U. Parlitz. *Int. J. Bif. Chaos*, 2:709, 1992.

[44] T. L. Carroll and L. M. Pecora. *Physica D*, 67:126, 1993.

[45] U. Parlitz, L. Junge, and L. Kocarev. *Phys. Rev. E*, 54:6253, 1996.

[46] J. Arnhold, P. Grassberger, K. Lehnertz, and C. E. Elger. *Physica D*, 134:419, 1999.

[47] R. Q. Quiroga, J. Arnhold, and P. Grassberger. *Phys. Rev. E*, 61:5142, 2000.

[48] A. Schmitz. *Phys. Rev. E*, 62:7508, 2000.

[49] S. J. Schiff, P. So, T. Chang, R. E. Burke, and T. Sauer. *Phys. Rev. E*, 54:6708, 1996.

[50] M. Wiesenfeldt, U. Parlitz, and W. Lauterborn. *Int. J. Bif. Chaos*, 11:2217, 2001.

[51] M. C. Romano, M. Thiel, J. Kurths, and W. von Bloh. *Phys. Lett. A*, 330:214, 2004.

[52] M. G. Rosenblum, A. S. Pikovsky, and J. Kurths. *Phys. Rev. Lett.*, 78:4193, 1997.

[53] L. Kocarev and U. Parlitz. *Phys. Rev. Lett.*, 76:1816, 1996.

[54] F. Takens. Detecting strange attractors in turbulence. In D. A. Rand and L.-S. Young, editors, *Dynamical Systems and Turbulence*, volume 898 of *Lecture Notes in Mathematics*. Springer, Berlin, 1980.

[55] H. Kantz and T. Schreiber. *Nonlinear Time Series Analysis*. Cambridge University Press, Cambridge, 1997.

[56] M. C. Romano, M. Thiel, J. Kurths, I. Z. Kiss, and J. Hudson. *Europhys. Lett.*, 71:466, 2005.

[57] D. Maraun and J. Kurths. *Geophys. Res. Lett.*, 32:15709, 2005.

[58] M. Palus. *Phys. Lett. A*, 235:341, 1997.

[59] M. Palus and A. Stefanovska. *Phys. Rev. E*, 67:055201(R), 2003.

[60] J. Theiler, S. Eubank, A. Longtin, B. Galdrikian, and J. D. Farmer. *Physica D*, 58:77, 1992.

[61] T. Schreiber and A. Schmitz. *Phys. Rev. Lett.*, 77:635, 1996.

[62] M. Small, D. Yu, and R. G. Harrison. *Phys. Rev. Lett.*, 87:188101, 2001.

[63] M. Thiel, M. C. Romano, J. Kurths, and R. Engbert. submitted.

[64] E. Ott. *Chaos in Dynamical Systems*. Cambridge University Press, Cambridge, 1993.

[65] E. Rodriguez et al. *Nature*, 397:430, 1999.

[66] C. Allefeld and J. Kurths. *Int. J. Bif. Chaos*, 14:405, 2004.

[67] Y. Kuramoto. *Chemical Oscillations, Waves and Turbulence*. Springer, New York, 1984.

[68] M. Peifer, B. Schelter, M. Winterhalder, and J. Timmer. *Phys. Rev. E*, 72: 026213, 2005.

[69] L. A. Riggs, F. Ratliff, J. C. Cornsweet, and T. N. Cornsweet. *J. Opt. Soc. Am.*, 43:495, 1953.

[70] D. Coppola and D. Purves. *Proc. Natl. Acad. Sci. USA*, 93:8001, 1996.

[71] R. Engbert and R. Kliegl. *Psychol. Science*, 15:431, 2004.

[72] K. J. Ciuffreda and B. Tannen. *Eye Movement Basics for the Clinician*. Mosby, St. Louis, 1995.

[73] W. Zhou and W. M. King. *Nature*, 393:692, 1998.

[74] D. L. Sparks. *Nature Rev. Neurosci.*, 3:952, 2002.

Index